RESEARCH ARTICLE

Key Points:
- LVOOA as the soluble organics reduces CCN overprediction
- Lower SS values are more sensitive to chemical composition and mixing state
- Changes in the composition are not represented by the O:C variation alone

Supporting Information:
- Readme
- Figure S1a
- Figure S1b
- Figure S2a
- Figure S2b
- Figure S2c
- Figure S2d
- Figure S2e
- Figure S2f
- Figure S2g
- Figure S2h
- Figure S2i
- Figure S2j
- Figure S3a
- Figure S3b
- Figure S3c
- Figure S3d
- Figure S3e
- Figure S3f
- Figure S3g
- Figure S4
- Figure S5
- Figure S6
- Figure S7
- Figure S8
- Figure S9
- Figure S10a
- Figure S10b
- Figure S10c

Correspondence to:
S. N. Tripathi,
snt@iitk.ac.in

CCN closure study: Effects of aerosol chemical composition and mixing state

Deepika Bhattu[1] and S. N. Tripathi[1,2]

[1]Department of Civil Engineering, Indian Institute of Technology Kanpur, Uttar Pradesh, India, [2]Centre for Environmental Science and Engineering, Indian Institute of Technology Kanpur, Uttar Pradesh, India

Abstract This study presents a detailed cloud condensation nuclei (CCN) closure study that investigates the effects of chemical composition (bulk and size resolved) and mixing state (internal and external) on CCN activity of aerosols. Measurements of the chemical composition, aerosol size distribution, total number concentration, and CCN concentration at supersaturation (SS = 0.2–1.0%) were performed during the winter season in Kanpur, India. Among the two cases considered here, better closure results are obtained for case 1 (low total aerosol loading, 49.54 ± 26.42 μg m^{-3}, and high O:C ratio, 0.61 ± 0.07) compared to case 2 (high total aerosol loading, 101.05 ± 18.73 μg m^{-3}, and low O:C ratio, 0.42 ± 0.06), with a maximum reduction of 3–81% in CCN overprediction for all depleted SS values (0.18–0.60%). Including the assumption that less volatile oxidized organic aerosols represent the soluble organic fraction reduced the overprediction to at most 40% and 129% in the internal and external mixing scenarios, respectively. At higher depleted SS values (0.34–0.60%), size-resolved chemical composition with an internal mixing state performed well in CCN closure among all organic solubility scenarios. However, at a lower depleted SS value (0.18%), closure is found to be more sensitive to both the chemical composition and mixing state of aerosols. At higher SS values, information on the solubility of organics and size-resolved chemical composition is required for accurate CCN predictions, whereas at lower SS values, information on the mixing state in addition to the solubility of organics and size-resolved chemical composition is required. Overall, κ_{total} values are observed to be independent of the O:C ratio [$\kappa_{total} = (0.36 \pm 0.01) \times$ O:C $- (0.03 \pm 0.01)$] in the range of 0.2<O:C<0.81, which indicates that the variation in the chemical composition of aerosols is not well represented by the changes in the O:C ratio alone.

1. Introduction

Atmospheric aerosols indirectly affect the global energy budget by acting as cloud condensation nuclei (CCN) [*Charlson et al.*, 1992]. The CCN activity of a particle strongly depends on the dry particle size, chemical composition, and mixing state [*McFiggans et al.*, 2006; *Dusek et al.*, 2006]. The Köhler theory provides a link between CCN activity and the hygroscopic growth of the aerosol. Because atmospheric aerosols are primarily complex mixtures of organics, inorganics, black carbon (BC), mineral dust, and sea salt, the multicomponent Köhler theory has been suggested to account for the effects of different solute species (mainly organics) on the surface tension [*Saxena and Hildemann*, 1996; *Petters and Kreidenweis*, 2007; *Wang et al.*, 2010]. Various laboratory studies have investigated organic compounds and inorganic-organic mixtures to understand the differences in their activation behavior, which arises primarily due to solubility, droplet surface tension, and effects on the mass accommodation coefficient of water. It is interesting to note that certain thermodynamically insoluble species also act as good CCN when present in metastable states or internally mixed with a small percentage of soluble species [*Chang et al.*, 2007]. Although organics constitute a major portion of aerosols (10–70% of the submicron mass of the ambient aerosols), their formation mechanisms, detailed speciation, and roles in influencing the Earth's radiation budget are still not well understood [*Saxena and Hildemann*, 1996; *Turpin et al.*, 2000; *Hallquist et al.*, 2009; *Kanakidou et al.*, 2005]. Recently, water-soluble organic compounds (WSOCs) have gained increased attention from researchers working on the indirect effect of aerosols. WSOCs are classified into hydrophilic and hydrophobic fractions depending on the number of carbon atoms and functional groups attached having a solubility greater than 1 g/100 g water [*Duarte and Duarte*, 2005; *Saxena and Hildemann*, 1996]. Hydrophilic compounds (e.g., saccharides, amines, and aliphatic monocarboxylic/dicarboxylic/oxocarboxylic acids) have short carbon chain compared to hydrophobic compounds (e.g., phenols and aromatic acids) [*Sullivan and Weber*, 2006]. Their atmospheric abundance and the ambiguous nature of their solubility,

density, and molecular weight poses a challenge in the quantification of spatial and temporal variations of CCN concentrations [*Chan et al.*, 2005; *McFiggans et al.*, 2006]. These compounds have the capability to affect the hygroscopicity of aerosols by depressing the surface tension and play important role in determining CCN activity of aerosols [*Novakov and Penner*, 1993]. It has been recently investigated that the contribution of WSOC in hygroscopicity is size dependent (varies with mass fraction of organic matter) [*Liu et al.*, 2014]. Hygroscopicity of the aerosols is represented by the ability of a particle to take up water, and it is quantitatively represented by a single parameter κ [*Petters and Kreidenweis*, 2007].

Despite extensive studies performed to investigate the effect of physical and chemical properties of aerosols on CCN activity, the level of detail for chemical composition and mixing state data required to achieve accurate CCN prediction is still debatable. Various CCN closure studies have achieved success within acceptable uncertainty levels ($\pm 20\%$) using a simplified chemical composition and internal mixing state for ambient aerosols [*Rissler et al.*, 2004; *Broekhuizen et al.*, 2006; *Wang et al.*, 2008; *Medina et al.*, 2007]. In the absence of information regarding chemical composition and mixing state, some studies have also demonstrated the use of aerosol hygroscopicity data from humidified tandem differential mobility analyzer (HTDMA) measurements in CCN closure [*Kammermann et al.*, 2010; *Kim et al.*, 2011]. These studies helped to assess the uncertainties associated with calculations assuming constant hygroscopicity under subsaturated and supersaturated conditions. A detailed description of previous CCN closure studies performed to understand the droplet activation of different types of aerosols is available in the literature [*Moore et al.*, 2013]. The success rates of the closure studies depend on the type of aerosols and meteorological conditions present. Furthermore, the treatment of aerosol chemical composition and mixing state in global models varies from highly sophisticated to simplified approaches. The realistic treatment of the aerosol mixing state in these models is important because it controls the effect of aerosol parameters (e.g., hygroscopicity) on CCN prediction [*Wang et al.*, 2010]. For example, the CCN activity of internally mixed aerosols is insensitive to the hygroscopicity of organics and is largely controlled by inorganic species [*Chang et al.*, 2010].

In the last few decades, sustained efforts have been made to understand the complex nature of organic aerosols (OAs) at the molecular level. These aerosols are mainly divided into two groups: primary organic aerosols (POAs) and secondary organic aerosols (SOAs). POAs are defined as organic compounds directly emitted into the atmosphere in particulate form or as vapors directly condensed on existing particles without undergoing gas phase transformations. In contrast, SOAs are formed by the atmospheric oxidation of gas phase species and represent up to 80% of the total organic aerosols in urban locations [*Zhang et al.*, 2007]. The rapidly evolving and transforming nature of organics in polluted urban and semiurban regions around the globe demand temporally resolved and size-resolved chemical composition measurements to account for the role of organic aerosols in CCN activity [*Jimenez et al.*, 2009; *Ng et al.*, 2011]. This need has been fulfilled by the advent of Aerodyne high-resolution-time-of-flight-aerosol mass spectrometer (HR-ToF-AMS). Furthermore, sources of organic aerosols can be characterized by positive matrix factorization (PMF) analysis of the AMS data set [*Paatero*, 1997]. Based on PMF analysis of the AMS data set, OAs are further speciated as less volatile oxidized organic aerosols (LVOOAs) and long-range transported biomass burning organic aerosols (LRT-BBOAs) representing the water-soluble fraction, while the water-insoluble fraction is represented by local or fresh emissions (HOA), such as traffic [*Timonen et al.*, 2013; *Xiao et al.*, 2011].

The objective of our study is to perform a CCN closure study of the ambient aerosols at an urban location, Kanpur, on the Indo-Gangetic Plain by comparing measured CCN concentrations with those predicted using the modified Köhler theory. Both ground- and aircraft-based closure studies have previously been performed at this location using filter-based chemical composition measurements [*Patidar et al.*, 2012; *Srivastava et al.*, 2013]. Additionally, the size-resolved CCN measurements have been performed over three different seasons to understand the effects of chemical composition on CCN activity [*Bhattu and Tripathi*, 2014]. To the best of our knowledge, this is the first AMS-based CCN closure study in India. In addition, the identification and characterization of submicron organic aerosol sources has been performed in this study. Previous CCN-based closure studies have been limited by assumptions regarding the solubility of organics, i.e., organics are assumed to be completely soluble, completely insoluble or to have defined fractions of soluble and insoluble components, which may not be applicable for urban locations [*Medina et al.*, 2007; *Broekhuizen et al.*, 2006; *Chang et al.*, 2007; *Srivastava et al.*, 2013]. WSOCs affect the CCN concentration by decreasing the critical diameter obtained from the Köhler theory. In addition to the solubility of organics, the co-condensation of organic vapors with water vapor has also been observed

to suppress activation supersaturation. This condensed mass increases under low-temperature and high relative humidity conditions and cannot be sampled under dry conditions at ground level [*Topping et al.*, 2013]. Even in highly polluted regions, lower concentrations of semivolatile gases and their diffusional losses inside the measurement system restrict the quantification of the increase in CCN potential due to the condensation of semivolatile products prior to cloud droplet formation in the atmosphere [*Romakkaniemi et al.*, 2014]. A recent study by *Romakkaniemi et al.* [2014] investigated the effects of inorganic semivolatile compounds on the CCN activity of aerosol particles by using a computational model for a droplet measurement technologies (DMT) CCN counter, a cloud parcel model for condensation kinetics. They found that the evaporation of ammonia and nitric acid from ammonium nitrate particles caused a 10–15 nm decrease in critical diameter at SS = 0.1–0.7%, whereas the condensation of nitric acid vapor increased the CCN potential only in the presence of high semivolatile compound concentrations in the gas phase.

The second objective of our study is to estimate the concentrations of water-soluble organics in the absence of real-time WSOC measurements and includes the results in this closure study. A CCN closure study by *Chang et al.* [2010] suggested the use of oxygenated factors, including soluble species, such as LVOOA, SVOOA, and BBOA, and insoluble species, such as HOA. Recent studies have compared real-time WSOC concentrations measured using particle-into-liquid sampler total organic carbon (PILS-TOC) data with the AMS-PMF-resolved factors, such as LVOOA, SVOOA, BBOA, and HOA. These studies have suggested that LVOOA and m/z 44 correlates well with WSOCs relative to other oxygenated factors [*Kondo et al.*, 2007; *Xiao et al.*, 2011; *Sun et al.*, 2011; *Timonen et al.*, 2013]. In this extended study, we used the AMS-PMF-resolved real-time LVOOA fraction as water-soluble organic aerosols to achieve CCN closure and better describe the hygroscopicity of the organic component of aerosols. The sensitivity of the CCN closure to chemical composition and mixing state is also investigated using different chemical composition and mixing state scenarios. The relationship between total hygroscopicity and the oxygen to carbon (O:C) ratio is also examined.

2. Experiment and Theory

The data presented here were collected during the winter season (7–27 November 2012) at the Centre for Environmental Science and Engineering (CESE) at the Indian Institute of Technology (IIT) Kanpur campus, India (26.5°N , 80.3°E, 125 m above mean sea level (AMSL)). Kanpur has a population of more than 4.5 million (1452 people/km^2), and the sampling site is located ~12 km northwest of the city center [*Kanawade et al.*, 2014]. The major pollution sources in the winter season are vehicle emissions, industrial emissions, biomass burning, open area burning, coal power plants, and domestic cooking [*Nair et al.*, 2007]. In addition, the site is also affected by long-range transported aerosols from the northwestern part of India, which experiences large numbers of forest fires [*Patidar et al.*, 2012]. The estimated distance of the fire hot spots (shown in Figure 1) from the sampling location is approximately 700–1000 Km. More details on the sampling location are provided elsewhere [*Ram et al.*, 2010a].

Measurements of the physical and chemical properties of submicron ambient aerosols were performed from the first floor of the CESE building at ~5 m above the ground. Dried ambient aerosols (relative humidity (RH) < 30% using a silica gel dryer) were sent to a TSI scanning mobility particle sizer (SMPS), DMT continuous-flow streamwise thermal-gradient CCN counter (CCN-100) and high resolution time-of-flight aerosol mass spectrometer (HR-ToF-AMS) to measure the aerosol size distribution, CCN concentration, and chemical composition, respectively. The aerosol size distribution (dN/dlogD_p) in the range of 14.6 nm to 680 nm was measured every 3 min with the SMPS. The sheath to aerosol ratio (SAR) was maintained at 10:1 during the sampling period. The CCN concentration (CCN, #/cc) was measured every second using the CCN counter at a flow rate of 0.5 Lpm and an SAR of 10:1 [*Roberts and Nenes*, 2005]. Prior to sampling, the CCN counter was calibrated using pure ammonium sulfate monodispersed aerosols (purity: >99%, Fischer Scientific). The details of the calibration procedure are provided elsewhere [*Bhattu and Tripathi*, 2014; *Rose et al.*, 2008]. The CCN measurements were performed at five SS values (0.2% (10 min), 0.4% (5 min), 0.6% (5 min), 0.8% (5 min), and 1% (5 min)). The ambient relative humidity (RH) and temperature were measured using a Vaisala temperature and RH sensor (Vaisala, Inc. Humicap, HMT 337, accuracy of ±1%).

HR-ToF-AMS (hereafter, AMS) was used to measure the aerosol chemical composition (nonrefractory species) at a vaporizer temperature of 600°C. The operational details of the AMS are described elsewhere [*DeCarlo et al.*, 2006]. AMS data included both the bulk and size-resolved mass of nonrefractory inorganic species as
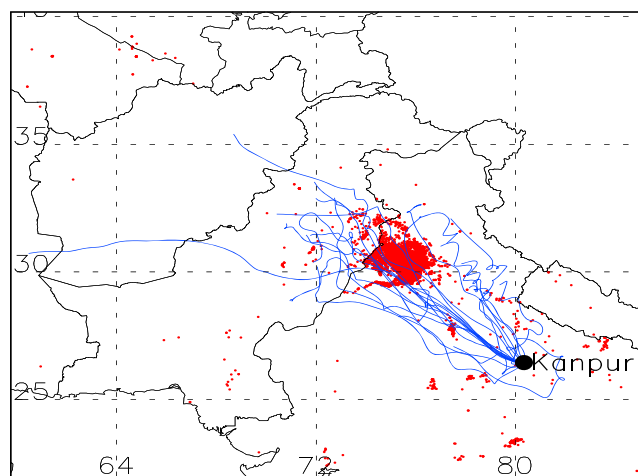
Figure 1. HYSPLIT back trajectory (1130 h Indian Standard Time (IST); 500 m) with MODIS fire count showing hot spots for 7–27 November 2012. The sampling period clearly features an air mass coming from the regions with fire activity (northwestern part of India).

well as total organic aerosols. The AMS was run alternatively in *V* and *W* modes (time-averaged mass resolution of 2903 and 4089 at m/z 184, respectively), each with 1 min sampling time. Due to a hard mirror malfunction, the *W*-mode data are not continuous. Therefore, the *V*-mode data are used in this study and include both mass spectrum (MS) and particle time-of-flight (PToF) measurements.

2.1. AMS Data Processing and PMF Analysis

The aerosol chemical composition (bulk and size resolved) was obtained using AMS [*DeCarlo et al.*, 2006; *Canagaratna et al.*, 2007]. The software package Igor Pro 6.22A (Wavemetrices) was used for the AMS data analysis (SQUIRREL v 1.52L, PIKA v 1.11L) [*Sueper et al.*, 2007]. The uncertainty in the AMS mass concentration measurements is due to the uncertainty involved in collection efficiency due to the bouncing of particles from the vaporizer surface, which varies with chemical composition. The chemically dependent collection efficiency (CE) was calculated to be 0.45 for our AMS data set [*Middlebrook et al.*, 2012]. Our results are not affected by the choice of CE because the CCN closure calculations involved only fractional chemical composition [*Chang et al.*, 2010]. Regular ionization efficiency (IE) calibrations were performed before, during, and after the experiment. The average relative ionization efficiency (RIE) for NH_4^+ was 4.6 during IE calibration, whereas the RIE for organics was assumed to be 1.4. The fraction of different species varied with particle size; therefore, the volume-fraction-weighted effective density of the particles for a particular size was calculated by assuming the typical densities for each of the major species present [*Kuwata et al.*, 2012]. The particle time of flight was calibrated using size-selected particles from a differential mobility analyzer (DMA, TSI). The duty cycle of the chopper and the PToF length were 2% and 0.395 m, respectively. Because the particle size measured by AMS represents the vacuum aerodynamic diameter and that measured by SMPS represents the mobility diameter, the vacuum aerodynamic diameter was converted to mobility diameter by dividing the value by the effective particle density, with the assumption of spherical particles [*DeCarlo et al.*, 2004]. This assumption is reasonable except for freshly emitted externally mixed BC aerosols. The mass size distribution obtained from AMS for all species is unimodal with a peak at approximately 500–600 nm, suggesting internally mixed aged aerosols, similar to other locations (Figure S1a in the supporting information) [*Takegawa et al.*, 2005]. The ratio of the inorganic to organic fraction with respect to size shows that small-sized particles contain most of the organics (Figure S1b).

In this study, PMF (Evaluation Tool v 2.06) [*Ulbrich et al.*, 2009] analysis of high-resolution (HR) mass spectra (m/z 12–300, V mode) data was performed to quantify the oxygenated and unoxygenated components of organic aerosols [*Paatero*, 1997]. Hybrid Single-Particle Lagrangian Integrated Trajectory (HYSPLIT) air mass back trajectory analysis was performed in conjunction with the global monthly Fire Location Product (MCD14ML) from Moderate Resolution Imaging Spectroradiometer (MODIS), which was obtained via the University of Maryland FTP server (ftp://fuoco.geog.umd.edu). Figure 1 shows that the fire counts during the sampling period were mainly concentrated in the northwestern part of India. The back trajectory analysis at 500 m shows that for most of the time, air masses also came from that region. The HR-PMF analysis was performed for one to eight factors to find the optimal solution. *f*Peak parameter (rotational values) varied from −2 to +2 with an interval of 0.2, corresponding to a maximum relative change of 3% in *Q/Q*exp graph. Different initialization seed values (random initial values) were explored from 1 to 30. A seven-factor solution (*f*Peak = 0) described the different sources on the basis of the factor profiles, time series, and their correlation with external factors. For *f*Peak values greater or less than 0, a solution was not chosen because it did not improve the correlation with external factors. The seven-factor solution

was found to be an optimal solution because solutions with a greater number of factors exhibited splitting behavior (Figure S2). A number of criteria, such as low Q/Qexp and higher correlation with external factors, were used in the selection of the optimal solution [*Ulbrich et al.*, 2009]. The fraction of total organics in different profile factors did not change much with the seed value, suggesting the robustness of our PMF solution (Figure S2). The total OAs measured by the AMS were resolved into seven factors: hydrocarbon-like OA (HOA), oxidized primary organic aerosols (OPOAs), less volatile oxidized OA (LVOOA), two types of semivolatile oxidized OA (SVOOA: more oxidized: SVOOA-1 and less oxidized: SVOOA-2), and two types of biomass burning OA (more oxidized: BBOA-2 and less oxidized: BBOA-1) (Figure S3). The LVOOA correlate well with m/z 44 measured by AMS (CO_2^+, $R^2 = 0.51$) and (SO_4^{2-}, $R^2 = 0.59$), whereas SVOOA-1 and SVOOA-2 correlate with NO_3^- ($R^2 = 0.2$ and 0.42, respectively) and HOA correlate with m/z 55 ($C_4H_7^+$) and m/z 57 ($C_4H_9^+$) ($R^2 = 0.59$ and 0.63, respectively). These characteristics are generally associated with fossil fuel combustion (Figure S4). The OPOA is characterized by f_{43} and f_{44}, with values of approximately 0.09 and 0.03, respectively. Similar values were obtained for the generation of SOA and OPOA using a potential aerosol mass flow reactor [*Lambe et al.*, 2011]. The OPOA O:C ratio is in the range 0.18–0.4, which was previously reported for primary biomass burning aerosols generated in the laboratory. The O:C ratio observed in ambient aerosols is less than 0.3–0.45, suggesting a contribution form primary biomass burning aerosols [*He et al.*, 2010, 2011]. Although we have found no diurnal peak representing COA, the relative peak intensity of m/z 55 is greater than that of m/z 57, which implies a contribution from cooking aerosols. The OPOA time series is similar to that of nitrate, m/z 55 and m/z 60, suggesting that the aerosols were not aged but originated from different POA sources (Figure S4). Earlier studies have also suggested that residual BBOA can accompany HOA in PMF analysis [*He et al.*, 2011]. We speculate that OPOA is a mixture of both biomass burning and cooking aerosols. The BBOA is identified by the markers at m/z 60 ($C_2H_4O_2^+$) and 73 ($C_3H_5O_2^+$) [*Aiken et al.*, 2009; *Cubison et al.*, 2011]. BBOA-1 and BBOA-2 are correlated with m/z 60 ($R^2 = 0.92$ and 0.33, respectively) and m/z 73 ($R^2 = 0.89$ and 0.38, respectively). The contributions of residual BBOA, cooking, trash burning, and slightly oxidized SOA have been shown to be difficult to separate; thus, it is not surprising that a contribution from m/z 60, which increases the O:C ratio, is present in HOA [*He et al.*, 2011; *Aiken et al.*, 2009]. Elemental O:C ratios for different profile factors were obtained after fitting peaks in HR data analysis. The limitations, accuracy, and precision in elemental analysis using HR-ToF-AMS have been discussed elsewhere [*Aiken et al.*, 2007, 2008].

2.2. CCN and Related Calculations

In this study, aerosols are considered to be composed of $(NH_4)_2SO_4$, NH_4NO_3, and organics. NO_3^- and SO_4^{2-} contributed up to 29% and 25% of the total aerosol composition, respectively. The speciation of ammonium sulfate salts depends on the molar ratio of ammonium to sulfate ions $R[SO_4]$ [*Nenes et al.*, 1998; *Asa-Awuku et al.*, 2011; *Padro et al.*, 2012]. If $R[SO_4] < 1$, the soluble fraction consists of a mixture of sulfuric acid and ammonium bisulfate; if $1 < R[SO_4] < 2$, the soluble fraction is a mixture of ammonium bisulfate and ammonium sulfate; and if $R[SO_4] > 2$, the soluble fraction consists of pure ammonium sulfate, as determined from the mass balance. $R[SO_4]$ is never less than unity which suggests that free sulfuric acid is not present in the aerosol system. A total of 84% of the data shows a molar ratio greater than 2, suggesting that pure ammonium sulfate is the best assumption for ammonium sulfate salts. Prior to averaging, CCN data are also removed for temperature transients (SS changes). The AMS and CCN data averaging time is kept same as the SMPS scan time, i.e., 3 min, thus eliminating 2 and 4 min of CCN data at the start of lower (0.2%) and higher (0.4%–1.0%) SS values, respectively. A supersaturation depletion correction has been applied due to high CCN concentrations following the same approach as described in earlier studies [*Lathem and Nenes*, 2011; *Patidar et al.*, 2012]. Hereafter, SS refers to depleted SS instead of measured SS. The multicomponent Köhler theory (equation (1)) is used to calculate the critical diameter assuming different mixing states (external and internal) and chemical composition (bulk and size resolved) as measured by AMS and the solubility of organics.

$$D_c = \left[\frac{256 M_w^3 \sigma^3}{27 R^3 T^3 \rho_w^3} \right]^{1/3} \left[\sum_i \left(\frac{M_w}{\rho_w} \right) \left[\left(\frac{\rho_i}{M_i} \right) \epsilon_i v_i \right] \right]^{-1/3} S^{-2/3} \qquad (1)$$

where S is supersaturation (%), M_w and ρ_w are molecular weight and density of water (0.01802 kg mol^{-1} and 1000 kg m^{-3}), and M_i and ρ_i are molecular weight and density of different solutes: $M_{(NH_4)_2SO_4} = 0.1321$ kg mol^{-1}, $M_{NH_4NO_3} = 0.08$ kg mol^{-1}, $M_{insoluble-organics} = 0.200$ kg mol^{-1}, $M_{soluble-organics} = 0.150$ kg mol^{-1},

Table 1. Average CCN Closure Ratios (Coefficient of Determination in Parenthesis) for Different Scenarios Obtained at the Different SS Levels (0.18–0.6%) Considered in This Study[a]

| | Bulk Composition | | | | | |
| | INT-ALLORG-SOL | | INT-LV-SOL | | INT-ALLORG-INSOL | |
SS (%)	1	2	1	2	1	2
$0.18 \pm 0.03\%$	1.83(0.53)	2.51(0.01)	1.59(0.52)	2.23(0.30)	1.47(0.44)	2.02(0.15)
$0.34 \pm 0.05\%$	1.47(0.88)	1.65(0.33)	1.37(0.87)	1.44(0.37)	1.28(0.82)	1.33(0.26)
$0.47 \pm 0.08\%$	1.35(0.91)	1.50(0.53)	1.28(0.90)	1.36(0.53)	1.22(0.88)	1.30(0.46)
$0.58 \pm 0.26\%$	1.34(0.89)	1.49(0.59)	1.29(0.88)	1.40(0.58)	1.29(0.88)	1.34(0.53)
$0.60 \pm 0.14\%$	1.25(0.81)	1.38(0.39)	1.23(0.84)	1.33(0.48)	1.13(0.76)	1.22(0.25)
	Bulk Composition					
	EXT-ALLORG-SOL		EXT-LV-SOL		EXT-ALLORG-INSOL	
	1	2	1	2	1	2
$0.18 \pm 0.03\%$	1.65(0.55)	2.46(0.25)	1.01(0.47)	1.17(0.12)	0.59(0.58)	0.74(0.06)
$0.34 \pm 0.05\%$	1.32(0.85)	1.53(0.38)	0.96(0.69)	0.77(0.06)	0.42(0.76)	0.39(0.25)
$0.47 \pm 0.08\%$	1.27(0.88)	1.41(0.52)	0.96(0.75)	0.78(0.05)	0.36(0.79)	0.33(0.20)
$0.58 \pm 0.26\%$	1.29(0.86)	1.43(0.58)	1.03(0.77)	0.85(0.07)	0.36(0.77)	0.33(0.32)
$0.60 \pm 0.14\%$	1.18(0.76)	1.32(0.34)	0.95(0.65)	0.84(0.06)	0.33(0.74)	0.30(0.29)
	Size-Resolved Composition					
	INT-ALLORG-SOL			INT-LV-SOL		
	1		2	1		2
$0.18 \pm 0.03\%$	1.68(0.48)		2.19(0.24)	1.51(0.35)		1.79(0.14)
$0.34 \pm 0.05\%$	1.37(0.83)		1.47(0.34)	1.35(0.58)		1.30(0.10)
$0.47 \pm 0.08\%$	1.28(0.87)		1.39(0.47)	1.27(0.72)		1.31(0.28)
$0.58 \pm 0.26\%$	1.29(0.86)		1.41(0.53)	1.28(0.76)		1.35(0.39)
$0.60 \pm 0.14\%$	1.14(0.70)		1.21(0.15)	1.12(0.52)		1.16(0.10)

[a]Here case 1 represents low total aerosol loading and high O:C ratios, whereas case 2 represents high total aerosol loading and low O:C ratios. The different scenarios include the following: internal mixing-all organics soluble (INT-ALLORG-SOL), internal mixing-LVOOA-soluble (INT-LV-SOL), internal mixing-all organics-insoluble (INT-ALLORG-INSOL), external mixing-all organics-soluble (EXT-ALLORG-SOL), external mixing-LVOOA-soluble (EXT-LV-SOL), and external mixing-all organics-insoluble (EXT-ALLORG-INSOL).

$\rho_{\text{insoluble-organics}} = 1000$ kg m^{-3}, $\rho_{(NH_4)_2SO_4} = 1760$ kg m^{-3}, $\rho_{NH_4NO_3} = 1720$ kg m^{-3}, ϵ_i is the volume fraction of solute; v_i is the van't Hoff factor of solute ($v_{\text{organics}} = 1$, $v_{(NH_4)_2SO_4} = 2.5$, $v_{NH_4NO_3} = 2$); T is ambient temperature (Kelvin); σ is the droplet surface tension, the same as that of pure water; and R is the gas constant (J K^{-1} mol^{-1}) [*Padro et al.*, 2012; *Moore et al.*, 2011]. The LVOOAs obtained from AMS-PMF analysis are the only soluble organic fraction considered throughout the closure study. The increase in the density of organics with solubility is due to a decrease in the molecular weight of soluble species. It is expected that hygroscopicity will change with the degree of aerosol oxygenation, which is due to changes in their intrinsic properties, such as molecular weight and density [*Chang et al.*, 2010; *Kuwata et al.*, 2012]. The density of LVOOA ($\rho_{\text{soluble-organics}} = 1465$ kg m^{-3}) is calculated by using O:C and H:C ratios [*Kuwata et al.*, 2012]. However, if all organics are considered to be soluble, the calculated $\rho_{\text{soluble-organics}}$ is 1290 kg m^{-3}.

To examine the relative importance of mixing state and chemical composition, eight different scenarios are used in our CCN closure study (Table 1). In the case of bulk chemical composition, the real-time (3 min averaged) volume fractions of different AMS-measured species, such as ammonium sulfate, ammonium nitrate, and LVOOA (representing the soluble organics), are used to calculate the critical diameter. In the case of size-resolved chemical composition, the real-time volume fractions of different species at a particular diameter are used in equation 1 to calculate the critical diameter. Here the relative contribution of LVOOA to total organics is multiplied by the real-time mass size distribution of organics to obtain the mass fraction of soluble organics, which is further divided by the density of LVOOA to obtain the volume fraction.

The aerosol size distribution obtained from SMPS is integrated above the critical diameter to calculate the CCN concentration (#/cc) using equation (2):

$$CCN = \int_{D_c}^{\infty} \left(\frac{dN}{d\log D_p} \right) dD_p \tag{2}$$

Furthermore, the hygroscopicity parameter (κ) for a dry particle at a particular supersaturation is calculated by using the κ-Köhler theory in which the water vapor saturation ratio over an aqueous droplet is given by equation (3) [*Petters and Kreidenweis*, 2007]:

$$s = \frac{D^3 - D_p^3}{D^3 - D_p^3(1-\kappa)} \exp \left(\frac{4\sigma_w M_w}{RT\rho_w D} \right) \tag{3}$$

where s is saturation ratio; D and D_p are the droplet wet diameter and particle dry diameter, respectively; and κ is a single parameter that combines specific properties (e.g., molecular weight, density, and van't Hoff factor) of the aerosols. This equation gives the total κ (κ_{total}) of aerosols for given values of critical SS (S_c) and D_p. However, κ_{org} is calculated by using a simple mixing rule, in which volume-weighted fractions of all participating species obtained via AMS are used (equation (4)):

$$\kappa_{total} = \epsilon_{inorg}\kappa_{inorg} + \epsilon_{org}\kappa_{org} \tag{4}$$

where ϵ_{inorg} and ϵ_{org} are the volume fractions of inorganics and organics, respectively [*Petters and Kreidenweis*, 2007]. Here κ_{inorg} includes $(NH_4)_2SO_4$ and NH_4NO_3 with hygroscopicity (κ) values of 0.61 and 0.67, respectively [*Wang et al.*, 2010].

3. Results and Discussion

The average time series and diurnal variation patterns of aerosol size distribution, the mass concentration of chemical species from AMS and CCN, and the CN number concentration are shown in Figures 2a–2f. The total aerosol concentration obtained from SMPS reaches 50,000 (#/cc), and the mode diameter ranges from 60 to 300 nm (Figure 2a). The mass size distribution obtained by AMS for all species is unimodal, with a peak at approximately 500–600 nm, suggesting that the particles are aged and of internally mixed nature (Figure S1a) [*Takegawa et al.*, 2005]. In the morning (0700–1000 h) and evening (1700–2000 h) traffic rush hours, the concentrations of Aitken-mode particles are high, which is consistent with HOA concentration (Figures 2a and 2c). In general, the particles emitted during evening hours continue to grow until the next morning, which is evident from the subsequently narrower size distribution and increased mode diameter (Figure 2a). After sunrise, the aerosol concentration decreases with increasing boundary layer height and dispersion of pollutants; this is observed on all days except 14–16, 25, and 26 November. The exceptions on these days could be due to the lower concentration of total aerosols, indicating a clean background air mass. The CCN concentration follows a similar pattern at different SS values ($0.18 \pm 0.03\%$, $0.34 \pm 0.05\%$, $0.47 \pm 0.08\%$, $0.58 \pm 0.26\%$, and $0.60 \pm 0.14\%$), with lower CN concentration and higher CCN/CN fraction during daytime (Figures 2d and S5). This trend is due to the presence of an aerosol size distribution with a larger mode diameter compared to that of other days. In addition, the CCN concentration at lower SS values ($0.18 \pm 0.03\%$) is less influenced by the peaks in CN. The CCN concentration ranges from 900 to 27,000 (#/cc) for all SS values (Figure 2d). The average ambient RH and temperature during the sampling period are $59 \pm 15\%$ and $19.1 \pm 3.5°C$ (Figure S6).

Large diurnal variations in aerosol properties are observed at the sampling site (Figures 2e and 2f). Both CCN and CN concentrations are lower around noon relative to nighttime. However, an opposite trend is observed in the O:C ratio, except for the morning rush hours, during which the competing effects of freshly emitted aerosols and photochemical activity can be observed (Figure 2f). Due to higher photochemical activity at noon, an increase in the most oxidized fraction of organics (LVOOA) causes an increase in the CCN concentration. The combined effect of both a lower CN concentration and higher O:C ratio at noon increases the CCN/CN fraction. Among the oxygenated factors, the LVOOA peak is shifted later in the day, possibly due to its photochemical production after sunrise (0620 h), as well as the temporal evolution of the boundary layer and the mixing of more oxidized aerosols from the residual layer above the nocturnal boundary layer. The diurnal pattern of LVOOA follows a trend similar to that of $(NH_4)_2SO_4$, which suggests the occurrence of photochemical production (Figure 2e). *Sun et al.* [2011] also observed a delay in the
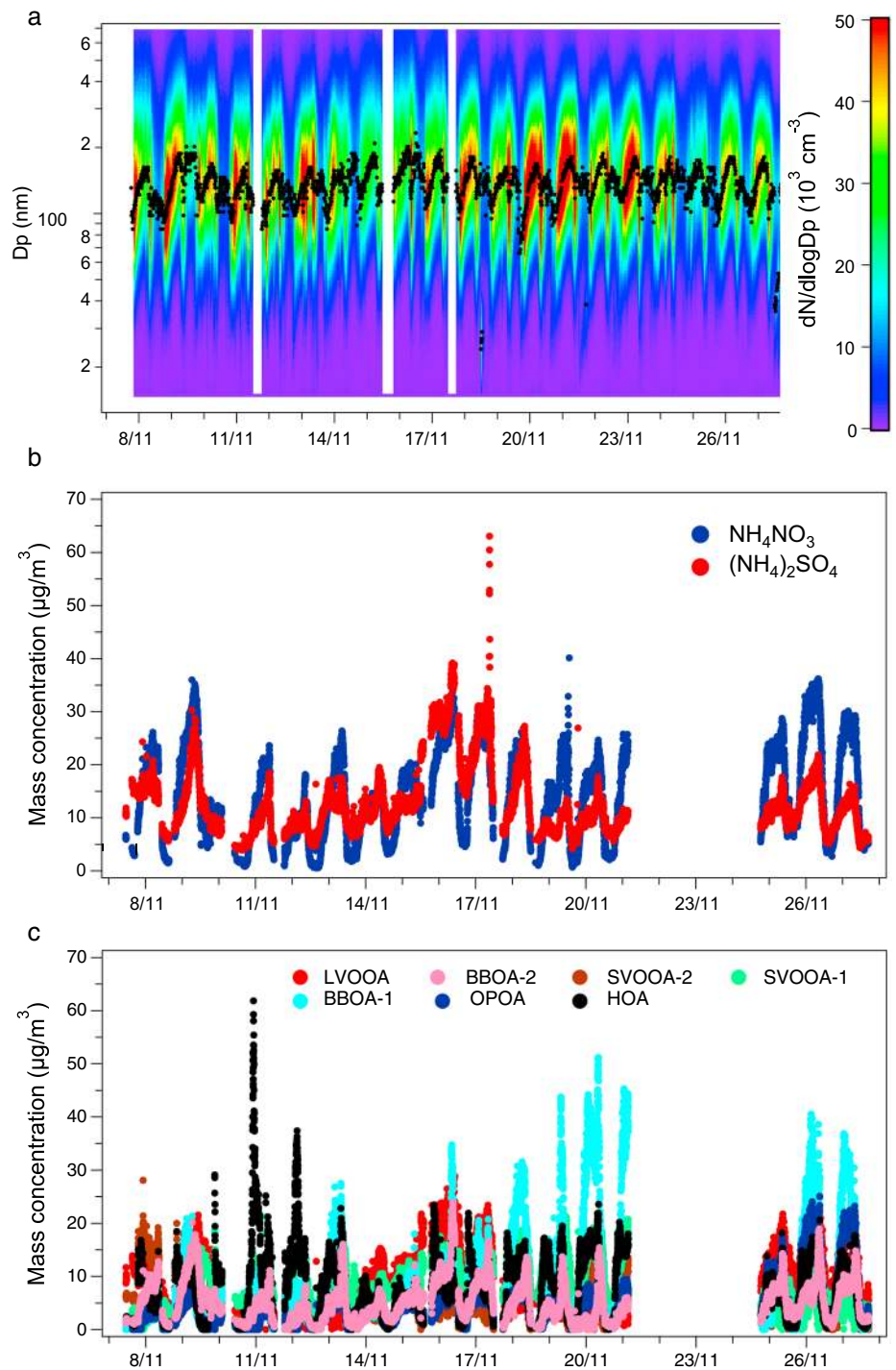
Figure 2. Time series of (a) SMPS size distribution with mode diameter represented by black dots; (b) bulk chemical composition of inorganics (($NH_4)_2SO_4$, NH_4NO_3) from HR-ToF-AMS; (c) organics including AMS-PMF-derived factors (LVOOA, SVOOA-1, SVOOA-2, BBOA-1, BBOA-2, OPOA, and HOA); and (d) CCN and CN concentrations (#/cc) at five different depleted SS values (0.18–0.60%), during the measurement period. (e and f) Diurnal variations of Figures 2b–2d with O:C ratios, respectively.
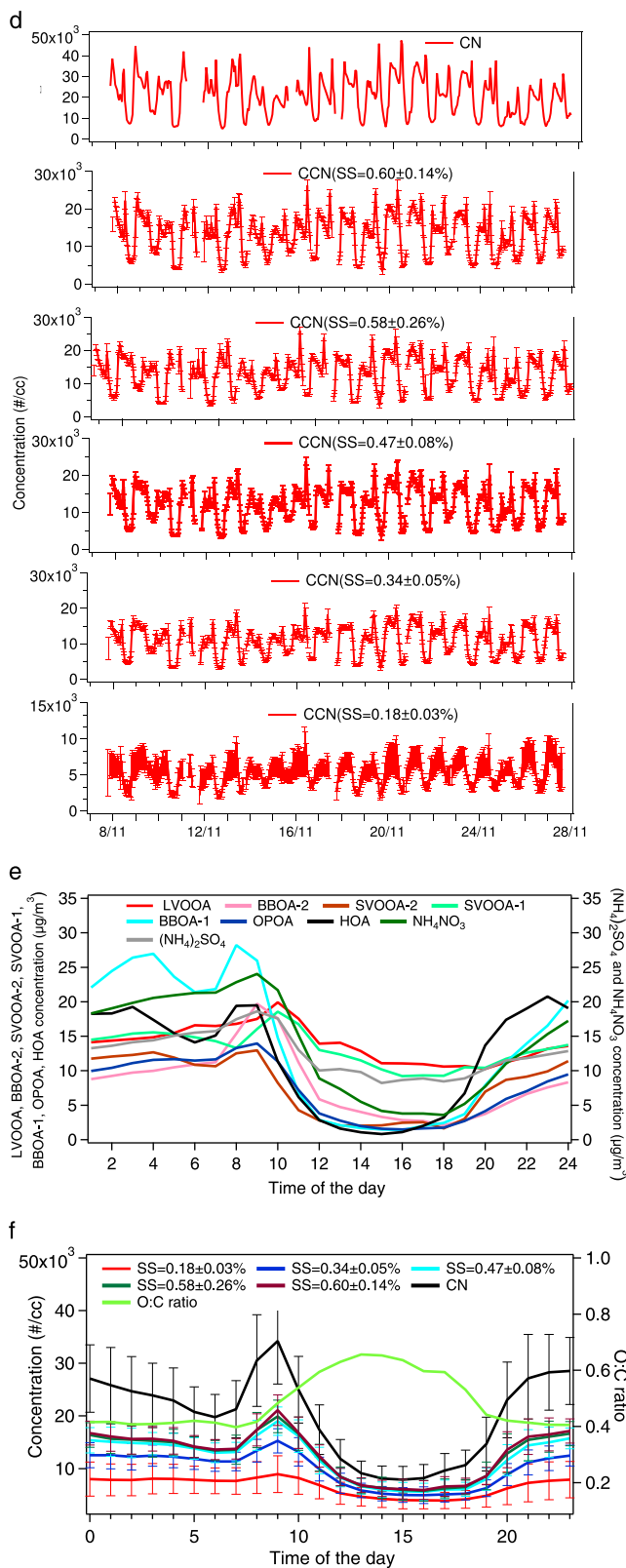
Figure 2. (continued)

photochemical production of LVOOA compared to sulfate and suggested that this delay is due to differences in their formation mechanisms. Additionally, maximum SOA concentrations observed in the afternoon on nonfoggy days are reported to be lower relative to evening concentrations on foggy days [*Kaul et al.*, 2011]. The diurnal pattern in BBOA and SVOOA concentrations is influenced by boundary layer activity, with BBOA concentrations being slightly higher in the night and morning hours and SVOOA concentrations being slightly higher in the evening hours (Figure 2e). Total OA, NH_4NO_3, and $(NH_4)_2SO_4$ concentrations range from 8.62 to 218.92, 0.54 to 40.13, and 3.88 to 63.04 $\mu g\ m^{-3}$, respectively. Higher NH_4NO_3 concentrations are observed at night compared to the day. This profile is likely due to gas-to-particle partitioning of its precursors, which allows the partitioning of HNO_3 to the particle phase under low temperature and higher RH conditions. In addition, NO_2 reacts with O_3 at night to form nitrate radicals, which are converted to nitric acid via thermal equilibrium with N_2O_5 (NO_3 radical pathway) [*DallOsto et al.*, 2009]. Although the formation of nitric acid via hydrolysis of N_2O_5 is very slow in the gas phase, the transformation can be rapid on aerosol particles via a heterogeneous process. However, the $(NH_4)_2SO_4$ concentration shows much less variation due to the opposing effects of an elevated boundary layer and higher SO_2 conversion rate. SO_2 is continuously emitted from thermal power plants and is converted to sulfate by photochemical activity and higher O_3 concentration (Figure 2e) [*Khoder*, 2002; *Ram et al.*, 2010b].

Because the contribution of organics to the total aerosol mass is ~75%, it is important to understand their sources, which can be either primary or secondary. The contribution of SVOOA to total OA is the greatest (up to 65.8%), followed by LVOOA

(up to 54%), BBOA (up to 53.8%), OPOA (up to 23.8%), and HOA (up to 7.5%). A higher HOA fraction ($\sim$22.6%) is observed during nighttime (1900–0100 h). To assess the aerosol acidity, the aerosol neutralization ratio is calculated from the molar ratio of $NH_{4(meas)}^{+}$ to $NH_{4(neu)}^{+}$ using AMS-derived chemical composition. The molar ratio of $NH_{4(meas)}^{+}$ is calculated as $NH_{4(meas)}^{+}/18$, and $NH_{4(neu)}^{+}$ is calculated as $2 \times [SO_4^{2-}]/96 + [NO_3^-]/62 + [Cl^-]/35.5$. The slope of $[NH_{4(meas)}^{+}]$ versus $[NH_{4(neu)}^{+}]$ is 0.99 ($R^2 = 0.97$). Approximately 96% of the data points are greater than unity indicating that aerosols are mostly neutralized during the sampling period.

3.1. CCN Closure and Its Sensitivity to Chemical Composition and Mixing State

A CCN closure study has been performed for the different scenarios listed in Table 1. The entire data set is further divided into two parts: low total aerosol loading with high O:C ratios (49.54 $\pm$ 26.42 µg m^{-3} and 0.61 $\pm$ 0.07, referred to as case 1) and high total aerosol loading with low O:C ratios (101.05 $\pm$ 18.73 µg m^{-3} and 0.42 $\pm$ 0.06, referred to as case 2). The data considered in cases 1 and 2 represent daytime (0900–1900 h) and nighttime (1900–0700 h), respectively. Our discussion is focused on these two cases to relate CCN predictions for distinct phases of aerosol chemical composition, mixing state, and atmospheric state, which is performed by comparing the predicted CCN with CCN values measured in different scenarios. The ratio of the average predicted CCN value to average measured CCN value is calculated, and the variation in the ratio is shown using the coefficient of determination. The different scenarios included are as follows:

1. Bulk composition-internal mixing-all organics-soluble (BULK-INT-ALLORG-SOL) scenario: All organics are assumed to be soluble, and all particles are assumed to be internally mixed in nature.
2. Bulk composition-internal mixing-LVOOA-soluble (BULK-INT-LV-SOL) scenario: All aerosols are assumed to be internally mixed, and only the LVOOA fraction of total organics is considered to be soluble.
3. Bulk composition-internal mixing-all organics-insoluble (BULK-INT-ALLORG-INSOL) scenario: All aerosols are assumed to be internally mixed, with organics treated as insoluble species.
4. Bulk composition-external mixing-all organics-soluble (BULK-EXT-ALLORG-SOL) scenario: The aerosols are externally mixed, and all organics are treated as soluble species. Additionally, each particle contains one of the following species: ammonium sulfate, ammonium nitrate, soluble organics, and insoluble organics.
5. Bulk composition-external mixing-LVOOA-soluble (BULK-EXT-LV-SOL) scenario: The aerosols are externally mixed, and the LVOOA fraction is the only soluble species among organics.
6. Bulk composition-external mixing-all organics-insoluble (BULK-EXT-ALLORG-INSOL) scenario: The organic species are completely insoluble and are externally mixed with all other considered species.
7. Size-resolved composition-internal mixing-all organics soluble (SR-INT-ALLORG-SOL) scenario: All size-resolved organics are assumed to be soluble, and all particles are assumed to be internally mixed in nature.
8. Size-resolved composition-internal mixing-LVOOA-soluble (SR-INT-LV-SOL) scenario: All aerosols are assumed to be internally mixed, and only the size-resolved LVOOA fraction of the total organics is considered to be soluble.

In CCN closure studies, the particle mixing state has generally been assumed to be independent of the size, which may not be strictly true because the mixing state changes with the time of the day, age of the aerosols, and distance from the potential source [*Wang et al.*, 2010]. The best CCN closure results are achieved in case 1 compared with case 2 in all the scenarios, possibly due to the presence of more aged aerosols, which are less affected by assumptions of chemical composition and mixing states (Table 1). A study conducted in Mexico City during Megacity Initiative: Local and Global Research Observations (MILAGRO, 2006) showed a similar pattern to that of case 2 in our study, in which the presence of POA and BC in the form of an external mixture deteriorated the closure ratio [*Wang et al.*, 2010]. Additionally, the sensitivity of CCN closure to other factors such as the solubility and surface tension of organics can lead to a poor closure ratio in periods with a low-soluble inorganic fraction (approximately 25% by total mass) [*Chang et al.*, 2007]. In contrast, another study at a high alpine site, Jungfraujoch (3580 m AMSL) in Switzerland, demonstrated that temporal variability in chemical composition can be neglected for CCN closure, even in the presence of a relatively high organic fraction ($\sim$45%) [*Juranyi et al.*, 2010].

The closure ratio obtained in all cases (cases 1 and 2) and scenarios shows a common pattern: the overprediction of CCN concentration decreases with increasing SS values. This suggests that higher SS values are less sensitive to chemical composition and mixing state. In general, as the solubility of organics shifts from entirely soluble organics (ALLORG-SOL) to only LVOOA are soluble (LV-SOL) to entirely insoluble organics (ALLORG-INSOL), the reductions in overprediction are highest (18–81%) at lower SS (0.18%). This pattern shows that at lower SS values, the solubility of organics plays an important role in the CCN activity
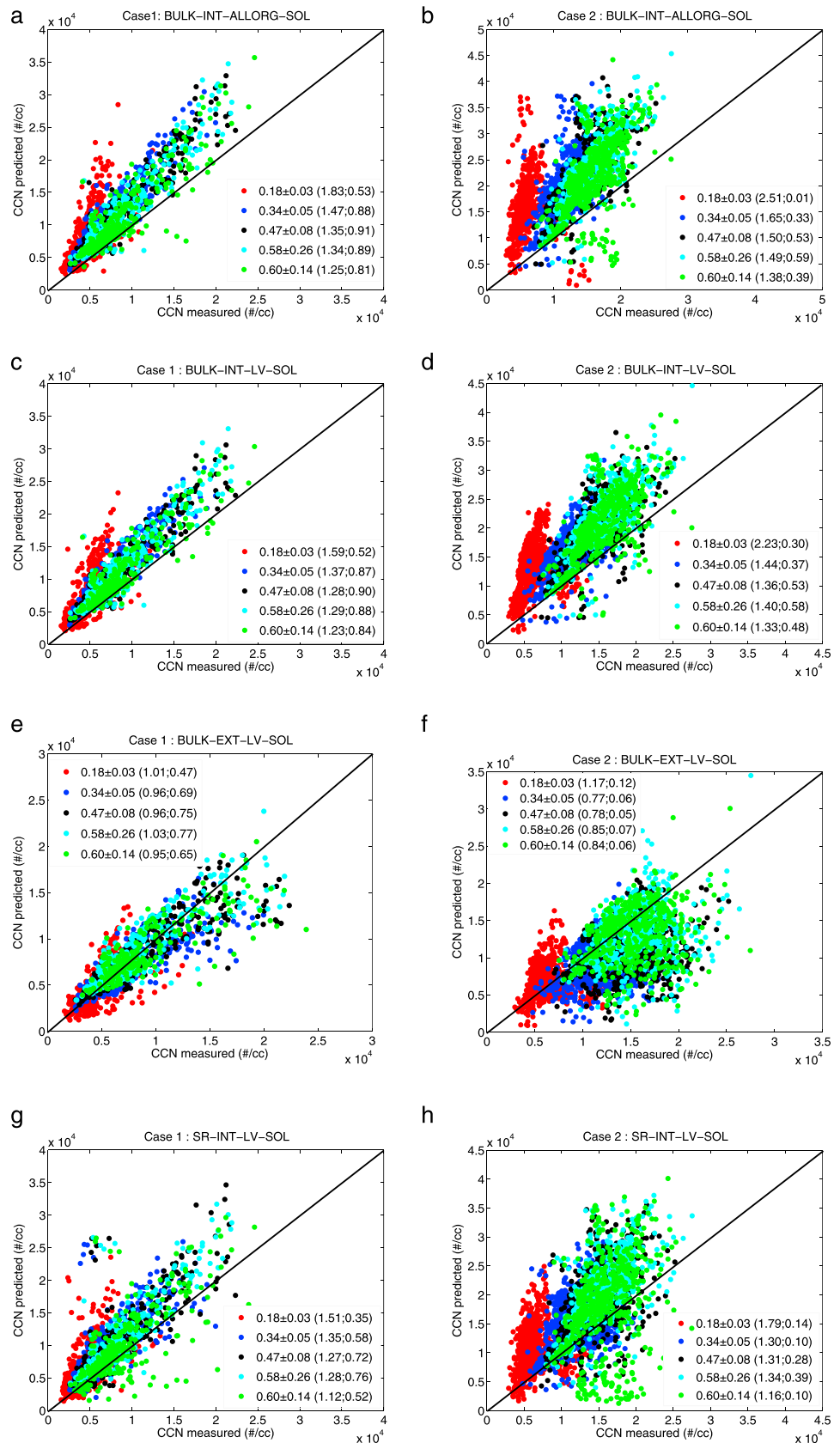
Figure 3

of aerosols, whereas at higher SS values, most particles become activated regardless of their chemical composition and size. Among the scenarios in which all organics are considered to be soluble (ALLORG-SOL), no mixing state effect is observed on the closure ratio. However, in scenarios in which the organics are completely insoluble (ALLORG-INSOL) or in which only LVOOA are soluble (LV-SOL), overprediction decreases by 80–128% and 28–106% when the assumed mixing state of the aerosols is changed from internally to externally mixed. Among the three internal mixing and bulk composition scenarios, BULK-INT-ALLORG-INSOL and BULK-INT-LV-SOL achieved better closure results, with 13–100% and 23–123% overprediction, respectively, compared to BULK-INT-ALLORG-SOL, with 25–151% overprediction (Table 1). Case 1 yields better closure results compared to case 2, with a maximum reduction in overprediction in the bulk composition and external mixing scenarios (3–81%), followed by bulk composition and internal mixing scenarios (9–68%) and size-resolved composition and internal mixing scenarios (4–51%) (Figures 3a–3h).

Among the bulk and size-resolved composition scenarios with internally mixed aerosols and entirely soluble organics (BULK-INT-ALLORG-SOL and SR-INT-ALLORG-SOL), overprediction is reduced in the SR-INT-ALLORG-SOL scenario by 7–15% in case 1 and by 11–32% in case 2. This result could be due to aerosol acidity, which increases with decreasing particle diameter (Figure S10a). Similar results have previously been attributed to the rapid condensation of sulfuric acid on smaller particles due to reduced diffusion limitations compared to larger particles [*Zhang et al.*, 2007]. In place of higher sulfate concentrations during acidic periods, we observe an increase in CHOgt1 mass concentration with increasing acidity (Figure S10b). The decrease in O:C ratio with increasing aerosol acidity in our study suggests that secondary organic acids are neutralized by the ammonia present in the aerosol phase (Figure S10c) [*Na et al.*, 2007]. Assuming all organics are soluble, no effect of size-resolved acidity is observed, whereas when only LVOOA are soluble (at higher diameter ranges), an effect of size-resolved acidity is observed. As reported earlier, *Zhang et al.* [2007] have also observed size-resolved acidity and studied its effect on SOA formation. Among the scenarios in which all organics are soluble (BULK-INT-ALLORG-SOL and BULK-EXT-ALLORG-SOL), the closure ratio improves by 5–18% and 6–12% in BULK-EXT-ALLORG-SOL in cases 1 and 2, respectively. The coefficient of determination also increased from 0.01 to 0.25 but only for a lower SS value of 0.18% (Table 1). These results suggest that the variation in the predicted CCN concentration is better correlated with measured CCN at lower SS values (0.18%) in BULK-EXT-ALLORG-SOL. However, LVOOA are the only soluble organics (BULK-INT-LV-SOL and BULK-EXT-LV-SOL); overprediction decreases in both case 1 and case 2. The variation in predicted CCN concentration is not better defined in case 2 due to low coefficients of determination (0.05–0.12) (Figures 3e and 3f). This suggests that the BULK-INT-LV-SOL scenario represents predicted CCN concentrations and their variation with measured concentration.

For an external mixture and bulk composition, BULK-EXT-ALLORG-INSOL shows an underprediction bias of 36–70%. Nevertheless, the remaining two scenarios (EXT-ALLORG-SOL and EXT-LV-SOL) feature overpredictions of 4–23% and 18–146%, respectively. It is worth noting that the solubility of organics significantly affects predicted CCN in both cases. A recent airborne study in regions influenced by industrial and urban sources also suggested that knowledge of the WSOC fraction combined with the assumption of internally mixed aerosols can significantly improve CCN closure [*Asa-Awuku et al.*, 2011].

Considering the longer lifetime of externally mixed aerosols, the better closure results obtained are unexpected because atmospheric processes, such as coagulation, gas condensation, and photochemical transformation, will shift these aerosols to an internally mixed state [*Moore et al.*, 2011; *De Gouw and Jimenez*, 2009; *Jimenez et al.*, 2009; *Shamjad et al.*, 2012]. Aerosol aging is defined as the change in chemical composition and particulate phase of aerosols via condensation, reactive uptake, or mass transfer processes [*Rudich et al.*, 2007]. It causes the production of secondary species, such as sulfate, nitrate, and SOA, and reduces the overall contribution of primary species, such as POA and BC, to the total aerosol volume. This reduction results in a reduced difference in predicted CCN concentration when using different mixing states for aged aerosols [*Wang et al.*, 2010; *Zhang et al.*, 2007; *Aggarwal and Kawamura*, 2009]. This finding

Figure 3. Comparison of predicted CCN with measured CCN for different scenarios considered in the study at five different supersaturation conditions (0.18% ($n = 2000$), 0.34% ($n = 1301$), 0.47% ($n = 1301$), 0.58% ($n = 980$), and 0.60% ($n = 978$)) for case 1 (low loading, high O:C ratios) and case 2 (high loading, low O:C ratios). Different assumptions involved are as follows: (a and b) BULK-INT-ALLORG-SOL, (c and d) BULK-INT-LV-SOL, (e and f) BULK-EXT-LV-SOL, and (g and h) SR-INT-LV-SOL. The average ratio and coefficient of determination (in parenthesis) of the predicted CCN relative to the measured CCN concentrations are shown in each plot. Here n = number of data points.

suggests that the implementation of an external mixing state is still valid in global models in the case of aged aerosols [*Textor et al.*, 2006]. Although an external mixing state provides better results, it does not represent real ambient conditions, which fall between external and internal mixing states. Therefore, we suggest that a simplified assumption of an internal mixing state combined with a size-resolved chemical composition can be used to reduce the CCN overprediction in conditions similar to case 1. However, in case 2 conditions, the presence of high HOA concentrations suggests that the assumption of an external mixing state is the best choice at lower SS values (0.18%). Furthermore, closures among the SR-INT-ALLORG-SOL and SR-INT-LV-SOL scenario, SR-INT-LV-SOL yield improved results, in which the predicted CCN concentration is only 12–79% greater than the measured one. It has been observed that the SR-INT-LV-SOL case yields improved closure in both cases 1 and 2 and at all supersaturations (Figures 3g and 3h). This all suggests that knowledge of the soluble organic fraction is required at higher SS values, but both the soluble organic fraction and mixing state are important for CCN prediction at lower SS values.

The presence of the higher HOA fraction (0.14 ± 0.03) in case 2, with a value twice that of case 1, suggests that particles are more externally mixed and remain in that state until they are mixed with other hygroscopic species, such as $(NH_4)_2SO_4$. It has previously been suggested that at a distance of 10 km from the emission source, CCN can be predicted well using simplified assumptions of a bulk chemical composition and an internal mixing state [*Wang et al.*, 2010]. Other studies have also observed externally mixed nonhygroscopic BC and HOA in evening hours. The mixing of HOA and BC with other hygroscopic species through coagulation in the absence of photochemistry is less effective than the condensation of secondary hygroscopic species in association with photochemistry [*Moffet et al.*, 2008; *Cross et al.*, 2009; *Wang et al.*, 2010]. Photochemical activity and the mixing and aging processes during long-range transport cause the particles to be more internally mixed during daytime. In addition, the presence of a relatively high volume fraction of inorganics in case 1 compared with case 2 results in reduced overprediction of CCN concentrations in case 1. The impact of a lower inorganic fraction on CCN closure, leading to uncertainties in CCN concentration and the hygroscopicity of aerosols, has already been examined [*Chang et al.*, 2007]. Our results suggest that more information on the aerosol's size-dependent mixing state is required for case 2 conditions to achieve closure ratios within uncertainty limits ($\pm20\%$). This is also consistent with previous studies that showed the need for both size-resolved chemical compositions and mixing states for better CCN closure during traffic hours due to the presence of freshly emitted HOA and BC [*Wang et al.*, 2010].

The sensitivity of CCN predictions to aerosol chemical composition and mixing state is further investigated with respect to time of day (Figure S7) to understand their relative importance compared with dynamic aerosol oxidation as a result of/via aging. At SS = 0.47–0.6% (first to third rows of Figure S7), the difference in the closure ratio in all three scenarios decreases during 1100–1800 h, which is consistent with the results in an earlier study [*Wang et al.*, 2010]. For the rest of the day, the predicted CCN is sensitive to mixing state and chemical composition, especially at lower SS value (0.18%, fifth row). Closure is improved for an external mixing state during nighttime and early morning hours because of the large fraction of HOA particles, which are mostly present in the Aitken mode size and do not contribute as CCN at the measured SS. At higher SS values (0.34–0.6%), detailed information about chemical composition improves closure.

3.2. Aerosol Hygroscopicity and Degree of Oxygenation

The parameter κ is calculated for the size-resolved chemical composition and INT-LV-SOL scenario, in which the best closure is achieved. Points lying outside the range $\mu \pm 3\sigma$ (where μ is the average and σ is the standard deviation) were removed before averaging. The average κ values calculated for cases 1 and 2 range between 0.01–0.35 and 0.01–0.32, respectively (with means of 0.20 and 0.12, respectively). These large variations are attributed to large variations in the volume fractions of inorganic species (Figure S8). The effect of aerosol chemical composition on the calculated hygroscopicity has also been observed. The calculated critical diameter for different SS values changes with changes in the chemical composition (Figure S9). The critical diameter increases as the soluble species decrease during the nighttime. The κ values obtained in this study are consistent with previous studies that considered mixtures of soluble salts and organic species but are lower than the values for continental aerosols ($\kappa = 0.3$) [*Padro et al.*, 2012; *Petters and Kreidenweis*, 2007; *Rose et al.*, 2010]. A size- and time-averaged κ value of 0.16 ± 0.08 was also observed over three different seasons, suggesting the dominance of organic aerosols [*Bhattu and Tripathi*, 2014]. It has been suggested that for κ values greater than 0.1, CCN closure can be achieved well within the uncertainty range ($\pm20\%$) by using simplified assumptions of chemical composition, i.e., bulk composition
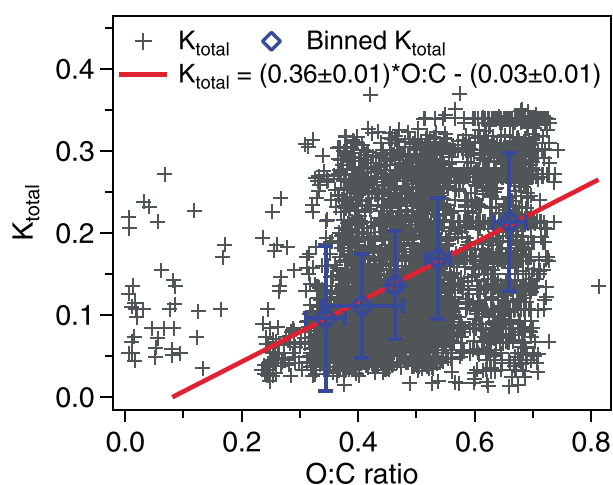
Figure 4. CCN-derived κ_{total} values as a function of the O:C ratio. The red line is fitted to the gray points. Blue markers are data points (mean ± 1 SD) binned by O:C ratio, with each bin representing a 20th percentile of the O:C ratio.

and mixing state, i.e., internal mixing [*Wang et al.*, 2010]. The κ values vary with the aging processes for different types of aerosols. They have a complex relationship as hygroscopicity can both increase (through oxidation) or decrease (through oligomerization) due to aging of organic aerosols [*Rudich et al.*, 2007]. A recent study showed that the κ value for anthropogenic industrial pollution is lowest (0.08 ± 0.01), followed by fresh and aged biomass burning aerosols (0.18 ± 0.13) and background aerosols (0.32 ± 0.21) [*Lathem et al.*, 2013]. The uncertainty involved in κ calculations could be due to the uncertainty caused by assuming that the surface tension is equal to that of water, which may not be the case when surfactants are present because of the combined effects of surfactants on surface partitioning and surface tension reductions in aqueous solution [*Chang et al.*, 2007; *Asa-Awuku et al.*, 2011]. A potential error analysis has been performed based on the uncertainty in CCN measurements. It has been observed that a 10% change in the effective SS can cause a ~40% change in calculations of the critical diameter. The effect of surfactants such as humic-like substances further depends on their dissolution and diffusion rates [*Taraniuk et al.*, 2007]. Several other factors contribute to potential uncertainties in κ, some of which have been listed in previous studies [*Chang et al.*, 2010]. Several past studies have successfully reconstructed the WSOC mass using oxygenated factors from AMS PMF analysis [*Xiao et al.*, 2011; *Timonen et al.*, 2013]. The factors obtained from PMF analysis were used in hygroscopicity calculations ($\kappa = 0.22$) by separating them into nonhygroscopic and unoxygenated (i.e., HOA) and hygroscopic and oxygenated (i.e., LVOOA, SVOOA, and BBOA) components [*Chang et al.*, 2010]. Recently, the hygroscopicity parameter obtained from size-resolved CCN measurements over the Kanpur region in India demonstrated the dominance of organics ($\kappa = 0.16$) and varying chemical composition with size [*Bhattu and Tripathi*, 2014]. In addition, in situ aircraft CCN measurement over Pantnagar and Gaya in India with a κ value of 0.5 also indicated the presence of moderately hygroscopic organic species with some inorganic content [*Srivastava et al.*, 2013].

The O:C ratio is the best representation of the degree of oxygenation [*Jimenez et al.*, 2009; *Aiken et al.*, 2008]. Even after considerable efforts, the dependence of aerosol hygroscopicity on the degree of oxygenation under subsaturated and supersaturated conditions is not well understood [*Jimenez et al.*, 2009; *Chang et al.*, 2010; *Juranyi et al.*, 2009]. A recent study by *Chang et al.* [2010] calculated the overall κ value to be 0.22 ± 0.04 using the O:C ratio for the organic fraction of aerosols. The dependence of hygroscopicity on the degree of oxygenation was confirmed, except for periods when aged continental aerosols were mixed with fresh traffic emissions. An empirical relationship was derived between κ_{org} and the O:C ratio assuming unoxygenated organic species to be completely nonhygroscopic [$\kappa_{org} = (0.9 \pm 0.5) \times$ O:C + (0.3 ± 0.2)]. A positive correlation between κ_{org} values and O:C ratios suggested the dependence of hygroscopicity on the degree of oxygenation of organic aerosols. A few field studies have shown both linear and nonlinear relationships between κ_{org} and O:C values under supersaturated and subsaturated RH conditions. The differences in the slopes were associated with the relative importance of nonideal interactions in dilute solutions near the point of CCN activation. In this study, Figure 4 shows κ_{total} values plotted as a function of O:C ratios. A slight correlation is observed between O:C ratios and κ_{total} values [$\kappa_{total} = (0.36 \pm 0.01) \times$ O:C − (0.03 ± 0.01)]. Because κ_{org} is not strongly correlated to the changes in the O:C ratio, the results suggest that other than the uncertainty due to the mixing state of aerosols, the chemical composition changes in a way that is not captured by variations in the O:C ratio [*Lathem et al.*, 2013]. We have found an increasing trend of κ_{total} with respect to O:C ratio for particles when κ_{total} values are binned by O:C ratio, with each bin representing a 20th percentile of the O:C ratio. This method has been used to remove the bias introduced due to the unequal number of points in each bin. Other studies have found a linear

correlation between κ_{org} and the O:C ratio ranging from 0.3 to 0.6 [*Chang et al.*, 2010; *Gunthe et al.*, 2009]. Here O:C ratios vary from 0.2 to 0.81 with an average of 0.49 ± 0.11. This value is quite similar to the values observed in Kaiping (near the Pearl River Delta region in South China), i.e., 0.47, which suggests the pollutants were highly oxidized [*Huang et al.*, 2011; *He et al.*, 2011]. An earlier study by *Moore et al.* [2011] observed that the increased organic oxygenation via the aging process increases the hygroscopicity up to values of 0.2–0.3; beyond these values hygroscopicity is less sensitive to O:C ratio. They also found low κ_{total} (0.15 ± 0.05) values similar to the values in this study even with a high O:C ratio, i.e., 1. It has been suggested that apart from the uncertainties due to mixing state and different aerosol sources, high O:C ratios and lower hygroscopicity are due to different secondary organic aerosol pathways than purely gas phase oxidation processes. The elemental O:C values obtained for the PMF factors were highest in LVOOA (1.02), followed by SVOOA-1 (0.76), BBOA-2 (0.58), SVOOA-2 (0.44), BBOA-1 (0.38), OPOA (0.23), and HOA (0.14). The high and low O:C ratios for BBOA suggest the presence of both fresh and aged biomass burning aerosols [*Timonen et al.*, 2013]. The long-range transport of BBOA is also supported by the air mass back trajectory analysis and fire counts (Figure 1).

4. Summary and Conclusions

A CCN closure study using HR-ToF-AMS was conducted in Kanpur, India, during the early winter season (November 2012). CCN concentrations measured at five different depleted supersaturation values (SS = 0.18–0.60%) were compared using the predicted by using modified Köhler theory, which involves different assumptions regarding the chemical composition (bulk and size resolved) of aerosols and their mixing state (external and internal). LVOOA obtained from AMS-PMF were used as the real-time concentration of water-soluble organic compounds (WSOCs). The conclusions derived from this study are as follows:

1. Case 1 (low total aerosol loading and high O:C ratios) yields better closure results than case 2 (high total aerosol loading and low O:C ratios) in all the scenarios considered in this study. Overall, overprediction is reduced in case 1 by 3–81% at SS values of 0.18–0.60% relative to case 2. Furthermore, the incorporation of LVOOA as soluble organics reduces the overprediction by up to 58% and 106% in cases 1 and 2, respectively. This suggests that knowledge of soluble organic fraction is important for improved closure results.
2. CCN closure is found to be more sensitive to chemical composition and mixing state at lower depleted SS values compared to higher SS values. The best closure results are obtained by using size-resolved chemical compositions and LVOOA as the soluble organic fraction. For case 2 conditions (with a higher HOA fraction), more information on the aerosol's size-dependent mixing state is required to achieve good closure results. As CCN closure results have been found to be dependent on the HOA/OA fraction, it has been suggested that if the HOA/OA fraction is less than 30%, CCN closure can be achieved within ±30% at SS values of >0.34%.
3. Bulk aerosols are found to be neutralized (the ratio of [$NH_{4(meas)}^+$] to [$NH_{4(neu)}^+$] is 0.99) during the sampling period, which suggests the presence of pure ammonium sulfate and ammonium nitrate as soluble inorganics. Additionally, both LVOOA and SVOOA represent the largest contributors to the total organics.
4. The correlation between the O:C ratio and κ_{total} values is determined to be $\kappa_{total} = (0.36 \pm 0.01) \times$ O:C $- (0.03 \pm 0.01)$. No correlation is observed between the κ_{org} and O:C ratios. These results show that the variation in the chemical composition of aerosols is not well represented by the changes in the O:C ratio alone. The average κ_{total} values for day and night are 0.20 and 0.12, respectively, which are consistent with previous studies performed done in organics-dominated regions.

In terms of the implications of this study for calculating the indirect effect of aerosols in global models, we have shown that the assumption of completely internally mixed aerosols will overestimate the predicted CCN in the presence of a higher fractional contribution of primary organic aerosols (HOA). Therefore, we need information on the size-resolved mixing state of aerosols to improve CCN predictions. Previous studies have shown the significance of particle size distribution relative to chemical composition, but our study suggests that particle chemical composition also needs to be evaluated, particularly in areas dominated by organics. Further studies on the Indian subcontinent are required to test the widely applicable relationship of hygroscopicity with the degree of oxygenation of organic aerosols. This information will be helpful in establishing empirical hygroscopicity relationships for climate models.

References

Aggarwal, S. G., and K. Kawamura (2009), Carbonaceous and inorganic composition in long-range transported aerosols over northern Japan: Implication for aging of water-soluble organic fraction, *Atmos. Environ.*, *43*(16), 2532–2540.

Aiken, A. C., P. F. DeCarlo and J. L. Jimenez (2007), Elemental analysis of organic species with electron ionization high-resolution mass spectrometry, *Anal. Chem.*, *79*(21), 8350–8358.

Aiken, A. C., et al. (2008), O/C and OM/OC ratios of primary, secondary, and ambient organic aerosols with high-resolution time-of-flight aerosol mass spectrometry, *Environ. Sci. Technol.*, *42*(12), 4478–4485.

Aiken, A. C., et al. (2009), Mexico City aerosol analysis during MILAGRO using high resolution aerosol mass spectrometry at the urban supersite (T0) Part 1: Fine particle composition and organic source apportionment, *Atmos. Chem. Phys.*, *9*(17), 6633–6653.

Asa-Awuku, A., et al. (2011), Airborne cloud condensation nuclei measurements during the 2006 Texas Air Quality Study, *J. Geophys. Res.*, *116*, D11201, doi:10.1029/2010JD014874.

Bhattu, D., and S. N. Tripathi (2014), Inter-seasonal variability in size-resolved CCN properties at Kanpur, India, *Atmos. Environ.*, *85*, 161–168.

Broekhuizen, K., R. Y. W. Chang, W. R. Leaitch, S. M. Li, and J. P. D. Abbatt (2006), Closure between measured and modeled cloud condensation nuclei (CCN) using size-resolved aerosol compositions in downtown Toronto, *Atmos. Chem. Phys.*, *6*(9), 2513–2524.

Canagaratna, M. R., et al. (2007), Chemical and microphysical characterization of ambient aerosols with the aerodyne aerosol mass spectrometer, *Mass Spectrom. Rev.*, *26*(2), 185–222.

Chan, M. N., M. Y. Choi, N. L. Ng, and C. K. Chan (2005), Hygroscopicity of water-soluble organic compounds in atmospheric aerosols: Amino acids and biomass burning derived organic species, *Environ. Sci. Technol.*, *39*(6), 1555–1562.

Chang, R. Y. W., P. S. K. Liu, W. R. Leaitch, and J. P. D. Abbatt (2007), Comparison between measured and predicted CCN concentrations at Egbert, Ontario: Focus on the organic aerosol fraction at a semi-rural site, *Atmos. Environ.*, *41*(37), 8172–8182.

Chang, R. Y. W., J. G. Slowik, N. C. Shantz, A. Vlasenko, J. Liggio, S. J. Sjostedt, W. R. Leaitch, and J. P. D. Abbatt (2010), The hygroscopicity parameter (κ) of ambient organic aerosol at a field site subject to biogenic and anthropogenic influences: Relationship to degree of aerosol oxidation, *Atmos. Chem. Phys.*, *10*(11), 5047–5064.

Charlson, R. J., S. E. Schwartz, J. M. Hales, R. D. Cess, J. A. Coakley, J. E. Hansen, and D. J. Hofmann (1992), Climate forcing by anthropogenic aerosols, *Science*, *255*, 423–430.

Cross, E. S., T. B. Onasch, M. Canagaratna, J. T. Jayne, J. Kimmel, X. Y. Yu, M. L. Alexander, D. R. Worsnop, and P. Davidovits (2009), Single particle characterization using a light scattering module coupled to a time-of-flight aerosol mass spectrometer, *Atmos. Chem. Phys.*, *9*(20), 7769–7793.

Cubison, M. J., et al. (2011), Effects of aging on organic aerosol from open biomass burning smoke in aircraft and laboratory studies, *Atmos. Chem. Phys.*, *11*, 12,049–12,064.

DallOsto, M., R. M. Harrison, H. Coe, P. I. Williams, and J. D. Allan (2009), Real time chemical characterization of local and regional nitrate aerosols, *Atmos. Chem. Phys.*, *9*(11), 3709–3720.

DeCarlo, P. F., J. G. Slowik, D. R. Worsnop, P. Davidovits, and J. L. Jimenez (2004), Particle morphology and density characterization by combined mobility and aerodynamic diameter measurements. Part 1: Theory, *Aerosol Sci. Technol.*, *38*(12), 1185–1205.

DeCarlo, P. F., et al. (2006), Field-deployable, high-resolution, time-of-flight aerosol mass spectrometer, *Anal. Chem.*, *78*(24), 8281–8289.

De Gouw, J., and J. L. Jimenez (2009), Organic aerosols in the Earth's atmosphere, *Environ. Sci. Technol.*, *43*(20), 7614–7618.

Duarte, R. M. B., and A. C. Duarte (2005), Application of non-ionic solid sorbents (XAD Resins) for the isolation and fractionation of water-soluble organic compounds from atmospheric aerosols, *J. Atmos. Chem.*, *51*, 79–93.

Dusek, U., et al. (2006), Size matters more than chemistry for cloud-nucleating ability of aerosol particles, *Science*, *312*, 1375–1378.

Gunthe, S. S., et al. (2009), Cloud condensation nuclei in pristine tropical rainforest air of Amazonia: Size-resolved measurements and modeling of atmospheric aerosol composition and CCN activity, *Atmos. Chem. Phys.*, *9*(19), 7551–7575.

Hallquist, M., et al. (2009), The formation, properties and impact of secondary organic aerosol: Current and emerging issues, *Atmos. Chem. Phys.*, *9*(14), 5155–5236.

He, L. Y., Y. Lin, X. F. Huang, S. Guo, L. Xue, Q. Su, M. Hu, S. J. Luan, and Y. H. Zhang (2010), Characterization of high resolution aerosol mass spectra of primary organic aerosol emissions from Chinese cooking and biomass burning, *Atmos. Chem. Phys.*, *10*, 11,535–11,543.

He, L. Y., X. F. Huang, L. Xue, M. Hu, Y. Lin, J. Zheng, R. Zhang, and Y. H. Zhang (2011), Submicron aerosol analysis and organic source apportionment in an urban atmosphere in Pearl River Delta of China using high-resolution aerosol mass spectrometry, *J. Geophys. Res.*, *116*, D12304, doi:10.1029/2010JD014566.

Huang, X. F., et al. (2011), Characterization of submicron aerosols at a rural site in Pearl River Delta of China using an Aerodyne High-Resolution Aerosol Mass Spectrometer, *Atmos. Chem. Phys.*, *11*(5), 1865–1877.

Jimenez, J. L., et al. (2009), Evolution of organic aerosols in the atmosphere, *Science*, *326*(5959), 1525–1529.

Juranyi, Z., et al. (2009), Influence of gas-to-particle partitioning on the hygroscopic and droplet activation behaviour of [small alpha]-pinene secondary organic aerosol, *Phys. Chem. Chem. Phys.*, *11*, 8091–8097.

Juranyi, Z., M. Gysel, E. Weingartner, P. F. DeCarlo, L. Kammermann, and U. Baltensperger (2010), Measured and modelled cloud condensation nuclei number concentration at the high alpine site Jungfraujoch, *Atmos. Chem. Phys.*, *10*(16), 7891–7906.

Kammermann, L., M. Gysel, E. Weingartner, H. Herich, D. J. Cziczo, T. Holst, B. Svenningsson, A. Arneth, and U. Baltensperger (2010), Subarctic atmospheric aerosol composition: 3. Measured and modeled properties of cloud condensation nuclei, *J. Geophys. Res.*, *115*, D04202, doi:10.1029/2009JD012447.

Kanakidou, M., et al. (2005), Organic aerosol and global climate modelling: A review, *Atmos. Chem. Phys.*, *5*(4), 1053–1123.

Kanawade, V. P., S. N. Tripathi, D. Singh, A. S. Gautam, A. K. Srivastava, A. K. Kamra, V. K. Soni, and V. Sethi (2014), Observations of new particle formation at two distinct Indian subcontinental urban locations, *Atmos. Environ.*, *96*, 370–379.

Kaul, D. S., T. Gupta, S. N. Tripathi, V. Tare, and J. L. Collett (2011), Secondary organic aerosol: A comparison between foggy and nonfoggy days, *Environ. Sci. Technol.*, *45*(17), 7307–7313.

Khoder, M. I. (2002), Atmospheric conversion of sulfur dioxide to particulate sulfate and nitrogen dioxide to particulate nitrate and gaseous nitric acid in an urban area, *Chemosphere*, *49*(6), 675–684.

Kim, J. H., S. S. Yum, S. Shim, S. C. Yoon, J. G. Hudson, J. Park, and S. J. Lee (2011), On aerosol hygroscopicity, cloud condensation nuclei (CCN) spectra and critical supersaturation measured at two remote islands of Korea between 2006 and 2009, *Atmos. Chem. Phys.*, *11*(24), 12,627–12,645.

Kondo, Y., Y. Miyazaki, N. Takegawa, T. Miyakawa, R. J. Weber, J. L. Jimenez, Q. Zhang, and D. R. Worsnop (2007), Oxygenated and water-soluble organic aerosols in Tokyo, *J. Geophys. Res.*, *112*, D01203, doi:10.1029/2006JD007056.

Kuwata, M., S. R. Zorn, and S. T. Martin (2012), Using elemental ratios to predict the density of organic material composed of carbon, hydrogen, and oxygen, *Environ. Sci. Technol.*, *46*(2), 787–794.

Lambe, A. T., T. B. Onasch, P. Massoli, D. R. Croasdale, J. P. Wright, A. T. Ahern, L. R. Williams, D. R. Worsnop, W. H. Brune, and P. Davidovits (2011), Laboratory studies of the chemical composition and cloud condensation nuclei (CCN) activity of secondary organic aerosol (SOA) and oxidized primary organic aerosol (OPOA), *Atmos. Chem. Phys.*, 11, 8913–8928.

Lathem, T. L., and A. Nenes (2011), Water vapor depletion in the DMT continuous-flow CCN chamber: Effects on supersaturation and droplet growth, *Aerosol Sci. Technol.*, 45(5), 604–615.

Lathem, T. L., A. J. Beyersdorf, K. L. Thornhill, E. L. Winstead, M. J. Cubison, A. Hecobian, J. L. Jimenez, R. J. Weber, B. E. Anderson, and A. Nenes (2013), Analysis of CCN activity of Arctic aerosol and Canadian biomass burning during summer 2008, *Atmos. Chem. Phys.*, 13(5), 2735–2756.

Liu, H. J., C. S. Zhao, B. Nekat, N. Ma, A. Wiedensohler, D. van Pinxteren, G. Splinder, K. Muller, and H. Herrmann (2014), Aerosol hygroscopicity derived from size-segregated chemical composition and its parameterization in the North China Plain, *Atmos. Chem. Phys.*, 14, 2525–2539.

McFiggans, G., et al. (2006), The effect of physical and chemical aerosol properties on warm cloud droplet activation, *Atmos. Chem. Phys.*, 6, 2593–2649.

Medina, J., A. Nenes, R. E. P. Sotiropoulou, L. D. Cottrell, L. D. Ziemba, P. J. Beckman, and R. J. Griffin (2007), Cloud condensation nuclei closure during the International Consortium for Atmospheric Research on Transport and Transformation 2004 campaign: Effects of size-resolved composition, *J. Geophys. Res.*, 112, D10S31, doi:10.1029/2006JD007588.

Middlebrook, A. M., R. Bahreini, J. L. Jimenez, and M. R. Canagaratna (2012), Evaluation of composition-dependent collection efficiencies for the aerodyne aerosol mass spectrometer using field data, *Aerosol Sci. Technol.*, 46(3), 258–271.

Moffet, R. C., B. de Foy, L. T. Molina, M. J. Molina, and K. A. Prather (2008), Measurement of ambient aerosols in northern Mexico City by single particle mass spectrometry, *Atmos. Chem. Phys.*, 8(16), 4499–4516.

Moore, R. H., R. Bahreini, C. A. Brock, K. D. Froyd, J. Cozic, J. S. Holloway, A. M. Middlebrook, D. M. Murphy, and A. Nenes (2011), Hygroscopicity and composition of Alaskan Arctic CCN during April 2008, *Atmos. Chem. Phys.*, 11(22), 11,807–11,825.

Moore, R. H., V. A. Karydis, S. L. Capps, T. L. Lathem, and A. Nenes (2013), Droplet number uncertainties associated with CCN: An assessment using observations and a global model adjoint, *Atmos. Chem. Phys.*, 13, 4235–4251.

Na, K., C. Song, C. Switzer, and D. R. Cocker (2007), Effect of ammonia on secondary organic aerosol formation from α-pinene ozonolysis in dry and humid conditions, *Environ. Sci. Technol.*, 41(17), 6096–6102.

Nair, V. S., et al. (2007), Wintertime aerosol characteristics over the Indo-Gangetic Plain (IGP): Impacts of local boundary layer processes and long-range transport, *J. Geophys. Res.*, 112, D13205, doi:10.1029/2006JD008099.

Nenes, A., C. Pilinis, and S. N. Pandis (1998), A new thermodynamic model for multiphase multicomponent inorganic aerosols, *Aquat. Geochem.*, 4, 123–152.

Ng, N. L., M. R. Canagaratna, J. L. Jimenez, P. S. Chhabra, J. H. Seinfeld, and D. R. Worsnop (2011), Changes in organic aerosol composition with aging inferred from aerosol mass spectra, *Atmos. Chem. Phys.*, 11(13), 6465–6474.

Novakov, T., and J. E. Penner (1993), Large contribution of organic aerosols to cloud-condensation-nuclei concentrations, *Nature*, 365, 823–826.

Paatero, P. (1997), Least squares formulation of robust non-negative factor analysis, *Chemom. Intell. Lab. Syst.*, 37(1), 23–35.

Padro, L. T., R. H. Moore, X. Zhang, N. Rastogi, R. J. Weber, and A. Nenes (2012), Mixing state and compositional effects on CCN activity and droplet growth kinetics of size-resolved CCN in an urban environment, *Atmos. Chem. Phys.*, 12(21), 10,239–10,255.

Patidar, V., S. N. Tripathi, P. K. Bharti, and T. Gupta (2012), First surface measurement of cloud condensation nuclei over Kanpur, IGP: Role of long range transport, *Aerosol Sci. Technol.*, 46(9), 973–982.

Petters, M. D., and S. M. Kreidenweis (2007), A single parameter representation of hygroscopic growth and cloud condensation nucleus activity, *Atmos. Chem. Phys.*, 7(8), 1961–1971.

Ram, K., M. M. Sarin, and S. N. Tripathi (2010a), A 1 year record of carbonaceous aerosols from an urban site in the Indo-Gangetic Plain: Characterization, sources, and temporal variability, *J. Geophys. Res.*, 115, D24313, doi:10.1029/2010JD014188.

Ram, K., M. M. Sarin, and S. N. Tripathi (2010b), Inter-comparison of thermal and optical methods for determination of atmospheric black carbon and attenuation coefficient from an urban location in northern India, *Atmos. Res.*, 97, 335–342.

Rissler, J., E. Swietlicki, J. Zhou, G. Roberts, M. O. Andreae, L. V. Gatti, and P. Artaxo (2004), Physical properties of the sub-micrometer aerosol over the Amazon rain forest during the wet-to-dry season transition—Comparison of modeled and measured CCN concentrations, *Atmos. Chem. Phys.*, 4(8), 2119–2143.

Roberts, G. C., and A. Nenes (2005), A continuous-flow streamwise thermal-gradient CCN chamber for atmospheric measurements, *Aerosol Sci. Technol.*, 39(3), 206–221.

Romakkaniemi, S., A. Jaatinen, A. Laaksonen, A. Nenes, and T. Raatikainen (2014), Ammonium nitrate evaporation and nitric acid condensation in DMT CCN counters, *Atmos. Meas. Tech.*, 7, 1377–1384.

Rose, D., S. S. Gunthe, E. Mikhailov, G. P. Frank, U. Dusek, M. O. Andreae, and U. Poschl (2008), Calibration and measurement uncertainties of a continuous-flow cloud condensation nuclei counter (DMT-CCNC): CCN activation of ammonium sulfate and sodium chloride aerosol particles in theory and experiment, *Atmos. Chem. Phys.*, 8(5), 1153–1179.

Rose, D., A. Nowak, P. Achtert, A. Wiedensohler, M. Hu, M. Shao, Y. Zhang, M. O. Andreae, and U. Poschl (2010), Cloud condensation nuclei in polluted air and biomass burning smoke near the mega-city Guangzhou, China—Part 1: Size-resolved measurements and implications for the modeling of aerosol particle hygroscopicity and CCN activity, *Atmos. Chem. Phys.*, 10(7), 3365–3383.

Rudich, Y., N. M. Donahue, and T. F. Mentel (2007), Aging of organic aerosol: Bridging the gap between laboratory and field studies, *Annu. Rev. Phys. Chem.*, 58, 321–352.

Saxena, P., and L. M. Hildemann (1996), Water-soluble organics in atmospheric particles: A critical review of the literature and application of thermodynamics to identify candidate compounds, *J. Atmos. Chem.*, 24, 57–109.

Shamjad, P. M., S. N. Tripathi, S. G. Aggarwal, S. K. Mishra, M. Joshi, A. Khan, B. Sapra, and K. Ram (2012), Comparison of experimental and modeled absorption enhancement by Black Carbon (BC) cored polydisperse aerosols under hygroscopic conditions, *Environ. Sci. Technol.*, 46(15), 8082–8089.

Srivastava, M., S. N. Tripathi, A. K. Dwivedi, R. Dalai, D. Bhattu, P. K. Bharti, J. Jaidevi, and T. Gupta (2013), CCN closure results from Indian Continental Tropical Convergence Zone (CTCZ) aircraft experiment, *Atmos. Res.*, 132-133, 322–331.

Sueper, D. T., J. Allan, E. Dunlea, J. Crosier, J. Kimmel, P. DeCarlo, A. C. Aiken, and J. L. Jimenez (2007), A community software for quality control and analysis of data from the aerodyne time-of-flight aerosol mass spectrometers (ToF-AMS), *2007 Annual Conference of the American Association for Aerosol Research*, Reno, Nev.

Sullivan, A. P., and R. J. Weber (2006), Chemical characterization of the ambient organic aerosol soluble in water: 1. Isolation of hydrophobic and hydrophilic fractions with a XAD-8 resin, *J. Geophys. Res.*, 111, D05314, doi:10.1029/2005JD006485.

Sun, Y. L., Q. Zhang, J. J. Schwab, W. N. Chen, M. S. Bae, Y. C. Lin, H. M. Hung, and K. L. Demerjian (2011), A case study of aerosol processing and evolution in summer in New York City, *Environ. Sci. Technol.*, *11*, 12,737–12,750.

Taraniuk, I., E. R. Graber, A. Kostinski, and Y. Rudich (2007), Surfactant properties of atmospheric and model humic-like substances (HULIS), *Geophys. Res. Lett.*, *34*, L16807, doi:10.1029/2007GL029576.

Takegawa, N., Y. Miyazaki, Y. Kondo, Y. Komazaki, T. Miyakawa, J. L. Jimenez, J. T. Jayne, D. R. Worsnop, J. D. Allan, and R. J. Weber (2005), Characterization of an Aerodyne Aerosol Mass Spectrometer (AMS): Intercomparison with other aerosol instruments, *Aerosol Sci. Technol.*, *39*(8), 760–770.

Textor, C., et al. (2006), Analysis and quantification of the diversities of aerosol life cycles within AeroCom, *Atmos. Chem. Phys.*, *6*(7), 1777–1813.

Timonen, H., et al. (2013), Characteristics, sources and water-solubility of ambient submicron organic aerosol in springtime in Helsinki, Finland, *J. Aerosol Sci.*, *56*, 61–77.

Topping, D., P. Connolly, and G. McFiggans (2013), Cloud droplet number enhanced by co-condensation of organic vapours, *Nat. Geosci.*, *6*, 443–446.

Turpin, B. J., P. Saxena, and E. Andrews (2000), Measuring and simulating particulate organics in the atmosphere: Problems and prospects, *Atmos. Environ.*, *34*(18), 2983–3013.

Ulbrich, I. M., M. R. Canagaratna, Q. Zhang, D. R. Worsnop, and J. L. Jimenez (2009), Interpretation of organic components from Positive Matrix Factorization of aerosol mass spectrometric data, *Atmos. Chem. Phys.*, *9*(9), 2891–2918.

Wang, J., Y. N. Lee, P. H. Daum, J. Jayne, and M. L. Alexander (2008), Effects of aerosol organics on cloud condensation nucleus (CCN) concentration and first indirect aerosol effect, *Atmos. Chem. Phys.*, *8*(21), 6325–6339.

Wang, J., M. J. Cubison, A. C. Aiken, J. L. Jimenez, and D. R. Collins (2010), The importance of aerosol mixing state and size-resolved composition on CCN concentration and the variation of the importance with atmospheric aging of aerosols, *Atmos. Chem. Phys.*, *10*(15), 7267–7283.

Xiao, R., et al. (2011), Characterization and source apportionment of submicron aerosol with aerosol mass spectrometer during the PRIDE-PRD 2006 campaign, *Atmos. Chem. Phys.*, *11*(14), 6911–6929.

Zhang, Q. I., J. L. Jimenez, D. R. Worsnop, and M. Canagaratna (2007), A case study of urban particle acidity and its influence on secondary organic aerosol, *Environ. Sci. Technol.*, *41*, 3213–3219.